Inference over Distribution of Posterior Class Probabilities for Reliable Bayesian Classification and Object-Level Perception

Vladimir Tchuiev and Vadim Indelman

***Abstract*—State of the art Bayesian classification approaches typically maintain a posterior distribution over possible classes given available sensor observations (images). Yet, while these approaches fuse all classifier outputs thus far, they do not provide any indication regarding how *reliable* the posterior classification is, thus limiting it's functionality in terms of autonomous systems and robotics. On the other hand, current deep learning based classifiers provide an uncertainty measure, thereby quantifying model uncertainty. However, they do so on a single frame basis and do not consider a sequential framework. In this paper we develop a novel approach that infers a distribution over posterior class probabilities, while accounting for model uncertainty. This distribution enables reasoning about uncertainty in the posterior classification, and therefore is of prime importance for robust classification, object-level perception in uncertain and ambiguous scenarios, and for safe autonomy in general. The distribution of the posterior class probability has no known analytical solution, thus we propose to approximate this distribution via sampling. We evaluate our approach in simulation and using real images fed into a convolutional neural network classifier.**

***Index Terms*—Deep Learning in Robotics and Automation; Recognition**

I. Introduction

CLASSIFICATION and object recognition is a fundamental problem in robotics and computer vision, which plays a significant role in numerous problem domains and applications, including semantic mapping, object-level SLAM, active perception and autonomous driving. Yet, reliable and robust classification in uncertain and ambiguous scenarios is challenging, as object classification is often viewpoint dependent, influenced by environmental visibility conditions such as lighting, clutter, image resolution and occlusions, and limited by the classifier's training set. In these challenging scenarios, classifier output can be sporadic and highly unreliable. Moreover, approaches that rely on most likely class observations can easily break, as these observations are treated equally regardless if the most likely class has high probability or not, potentially giving large significance to ambiguous observations.

Indeed, modern (deep learning based) classifiers provide much richer information that is being discarded by resorting to only most likely observations. Current convolutional neural network (CNN) classifiers provide not only vector of class probabilities (i.e. probability for each class), but, recently, also output an uncertainty measure, quantifying how (un)certain each of these probabilities is.

Even though CNN-based classification achieved remarkable results in the last few years, as with any data driven method, actual performance heavily depends on the training set. In particular, if the classified object is represented poorly in the training set, the classification result will be unreliable and vary greatly with slightly different classifier weights. This variation is referred to as model uncertainty. High model uncertainty tends to arise from input that is far from the classifier's training set, which could be caused by an object not being in the training set or by occlusions. In addition, classification, where each frame is treated separately, is influenced by environmental conditions such as lighting and occlusions. Consequently, it can provide unstable classification results. Various methods were proposed to compute model uncertainty from a single image (see [1]–[3]).

To address this problem, various Bayesian sequential classification algorithms (e.g. [4]–[10]) that maintain a posterior class distribution were developed; however, none of these approaches address model uncertainty. Crucially, while posterior class distribution fuses all classifier outputs thus far, it does not provide any indication regarding how reliable the posterior classification is. In Bayesian inference over continuous random variables (e.g. SLAM problem), this would correspond to getting the maximum a posteriori solution without providing the uncertainty covariances! Clearly, this is highly undesired, in particular in the context of *safe* autonomous decision making (e.g. in robotics, or for self driving cars), where a key question is *when* should a decision be made given available data thus far (see e.g. [11]). On the other hand, existing approaches that account for model uncertainty do not consider sequential classification. As a consequence, none of the existing approaches reason about the posterior uncertainty, given images thus far.

In this paper we address this gap and propose to maintain a *distribution over posterior class probabilities* while accounting for model uncertainty. This distribution enables reasoning about uncertainty in posterior classification, which is crucial for robust classification, and for safe autonomy in general. In particular, we derive equations to sequentially update the distribution over posterior class probabilities. We evaluate our approach in simulation, and using real images fed into a deep learning classifier.

Manuscript received: February 20th 2018; Revised May 17th 2018; Accepted June 18th 2018. This paper was recommended for publication by Editor Tamim Asfour upon evaluation of the Associate Editor and Reviewers' comments.

The authors are with the Department of Aerospace Engineering, Technion - Israel Institute of Technology, Haifa 32000, Israel, {vovatch, vadim.indelman}@technion.ac.il.

II. Related Work

Several sequential classification algorithms were developed in recent years. Coates and Y. Ng [4] proposed a method that updates posterior class probability by multiplying prior class probability with a new classification measurement, considering an object detection problem. Omidshafiei et al. [5] mention the Static State Bayes Filter (SSBF) algorithm that extends the work by Coats and Y. Ng for multiple possible classes. It assumes the prior, posterior and likelihood all categorically distributed. Patten et al. [10] used a method similar to SSBF in the context of active classification. Atanasov et al. [6] proposed a method that updates categorically distributed posterior pairs of candidate object classes and orientations. This approach utilizes a viewpoint dependent observation model. Omidshafiei et al. [5] developed the hierarchical Bayesian noise inference (HBNI) algorithm. At each time step, the algorithm updates class probabilities with the likelihood of the soft-max classifier output modeled by a Dirichlet distribution, with a noise parameter for each possible class. Mu et al. [7] utilizes a Dirichlet prior and most likely classifier observations, while addressing the challenging problem of data association.

Works by Teacy et al. [8] and Velez et al. [9] propose approaches that utilize a viewpoint dependent classifier model to update posterior class probability. Both works are presented in the context of active classification. While Velez et al. only consider correlation aspects of past observations, Teacy et al. also consider correlation aspects for future observations. Crucially, these approaches do not consider model uncertainty, i.e. how reliable is the classifier output.

Recently, several works developed methods for computing model uncertainty for deep learning applications. Grimmett et al. [12] suggested using normalized entropy of class probability as a measure of classification uncertainty. However that approach does not consider model uncertainty. Gal and Ghahramani [1] [2] proposed utilizing neural network dropout to estimate model uncertainty for an input of a single image. Kendal and Cipolla [13] build upon these works, utilizing dropout to compute uncertainty in CNN-based camera relocalization. Both infer model uncertainty from a single image input only. Further, Kendal and Gal [14] analyze the major two types of uncertainty: epistemic uncertainty or model uncertainty, and aleatoric uncertainty that captures noise inherent in observations. Mishkov and Julier [3] compare between multiple methods to predict uncertainty in classifier output, using Hybrid Monte Carlo (HMS) as a baseline. They found that Stochastic Gradient Langevin Dynamics (SGLD) and Dropout (see [2]) methods performed the best in terms of accuracy. Yet, these works consider classification given a single image frame, as opposed to Bayesian sequential classification given multiple images that we consider herein.

III. Notation and Problem Formulation

Consider a robot observing a single object from multiple viewpoints, aiming to infer its class while quantifying uncertainty in the latter. Each class probability vector is $\gamma_k \doteq \begin{bmatrix} \gamma_k^1 & \cdots & \gamma_k^i & \cdots & \gamma_k^M \end{bmatrix}$, where M is the number of candidate classes. Each element γ_k^i is the probability of object class c being i given image z_k, i.e. $\gamma_k^i \equiv \mathbb{P}(c = i|z_k)$, while γ_k resides in the $(M-1)$ simplex such that

$$\gamma_k^i \geqslant 0 \qquad ||\gamma_k||_1 = 1. \tag{1}$$

Existing Bayesian sequential classification approaches do not consider model uncertainty, and thus maintain a posterior distribution λ_k for time k over c,

$$\lambda_k \doteq \mathbb{P}(c|\gamma_{1:k}), \tag{2}$$

given history $\gamma_{1:k}$ obtained from images $z_{1:k}$. In other words, λ_k is inferred from a single sequence of $\gamma_{1:k}$, where each γ_t for $t \in [1, k]$ corresponds to an input image z_t. However, the posterior class probability λ_k by itself does not provide any information regarding how reliable the classification result is due to model uncertainty. For example, a classifier output γ_k may have a high score for a certain class, but if the input is far from the classifier training set the result is not reliable and may vary greatly with small changes in the scenario and classifier weights.

In this paper we wish to reason about model uncertainty, i.e. quantify how "far" an image input z_t is from the training set D by modeling the distribution $\mathbb{P}(\gamma_t|z_t, D)$. Given a training set D and classifier weights w, the output γ_t is a deterministic function of input z_t for all $t \in [1, k]$:

$$\gamma_t = f_w(z_t), \tag{3}$$

where the function f_w is a classifier with weights w. However, w are stochastic given D, thus inducing a probability $\mathbb{P}(w|D)$ and making γ_t a random variable. Gal and Ghahramani [2] showed that an input far from the training set will produce vastly different classifier outputs for small changes in weights. Unfortunately, $\mathbb{P}(w|D)$ is not given explicitly. To combat this issue, Gal and Ghahramani [2] proposed to approximate $\mathbb{P}(w|D)$ via dropout, i.e. sampling w from another distribution closest to $\mathbb{P}(w|D)$ in a sense of KL divergence. Practically, we run an input image z_t through a classifier with dropout multiple times to get many different γ_t's for corresponding w realizations, creating a point cloud of class probability vectors. Note that every distribution in this paper is dependent on the training set D, so we omit it from further expressions to avoid clutter.

In this paper, a class-dependent likelihood $\mathbb{P}(\gamma_k|c = i)$, referred as a classifier model, is utilized. We use a Dirichlet distributed classifier model with a different hyperparameter vector $\theta_i \in \mathbb{R}^{M \times 1}$ per class $i \in [1, M]$, rewriting $\mathbb{P}(\gamma_k|c = i)$ as:

$$\mathbb{P}(\gamma_k|c = i) = Dir(\gamma_k; \theta_i). \tag{4}$$

This distribution is the conjugate prior of the categorical distribution, thus it supports class probability vectors, particularly γ_k. Sampling from Dirichlet distribution necessarily satisfies conditions (1), unlike other distributions such as

Gaussian. The probability density function (PDF) of the above distribution is as follows:

$$Dir(\gamma_k;\theta_i) = C(\theta_i)\prod_{j=1}^{M}\left(\gamma_k^j\right)^{\theta_i^j-1}, \tag{5}$$

where $C(\theta_i)$ is a normalizing constant dependent on θ_i, and θ_i^j is the j-th element of vector θ_i. To shorten notation, we will write this likelihood as:

$$\mathbb{P}(\gamma_k|c=i) \doteq \mathcal{L}_i(\gamma_k), \qquad \mathbb{P}(\cdot|c=i) \doteq \mathcal{L}_i. \tag{6}$$

We denote the likelihood vector as $\mathcal{L}(\gamma_k) \doteq \left[\ \mathcal{L}_1(\gamma_k)\cdots\mathcal{L}_M(\gamma_k)\ \right]$. For simplicity, we consider these hyperparameter vectors to be known or inferred. Furthermore, in this paper we assume an uninformative prior $\mathbb{P}(c=i)=1/M$.

We must distinguish between the classifier model $\mathcal{L}_i(\gamma_k)$, and the model uncertainty derived from $\mathbb{P}(\gamma_k|z_k)$ for class i and time step k. The classifier model $\mathcal{L}_i(\gamma_k)$ is the likelihood of a single γ_k given a class hypothesis i; it is computed *prior to the scenario* for each class from the training set, and it is assumed constant within the scenario. On the other hand, $\mathbb{P}(\gamma_k|z_k)$ is the probability of γ_k given an image z_k, and is computed *during the scenario*. Note that if the true object class is i and it is "close" to the training set, the probabilities $\mathbb{P}(\gamma_k|z_k)$ and $\mathcal{L}_i(\gamma_k)$ will be "close" to each other as well.

A *key observation* is that λ_k is a random variable, as it depends on $\gamma_{1:k}$ (see Eq. (2)) while each γ_t, with $t\in[1,k]$, is a random variable distributed according to $\mathbb{P}(\gamma_t|z_t,D)$. Thus, rather than maintaining the posterior Eq. (2), our goal is to maintain a *distribution over posterior class probabilities* for time k, i.e.

$$\mathbb{P}(\lambda_k|z_{1:k}). \tag{7}$$

This distribution allows to calculate the posterior class distribution, $\mathbb{P}(c|z_{1:k})$, via expectation

$$\begin{aligned}\mathbb{P}(c=i|z_{1:k}) &= \int_{\lambda_k^i}\mathbb{P}(c=i|\lambda_k^i,z_{1:k})\mathbb{P}(\lambda_k^i|z_{1:k})d\lambda_k^i\\ &= \int_{\lambda_k^i}\mathbb{P}(c=i|\lambda_k^i)\mathbb{P}(\lambda_k^i|z_{1:k})d\lambda_k^i = \mathbb{E}[\lambda_k^i],\end{aligned} \tag{8}$$

where we utilized the identity $\mathbb{P}(c=i|\lambda_k^i)=\lambda_k^i$.

Moreover, as will be seen, Eq. (7) allows to quantify the *posterior uncertainty*, thereby providing a measure of confidence in the classification result given all data thus far.

At this point, it is useful to summarize our assumptions:

1) A single object is observed multiple times.
2) $\mathbb{P}(\gamma_t|z_t,D)$ is approximated by a point cloud $\{\gamma_t\}$ for each image z_t.
3) An uninformative prior for $\mathbb{P}(c=i)$.
4) A Dirichlet distributed classifier model with with designated parameters for each class $c\in[1,\ldots,M]$. These parameters are constant and given (e.g. learned).

IV. Approach

We aim to find a distribution over the posterior class probability vector λ_k for time k, i.e. $\mathbb{P}(\lambda_k|z_{1:k})$. First, λ_k is expressed given some specific sequence $\gamma_{1:k}$. Using Bayes' law:

$$\lambda_k^i = \mathbb{P}(c=i|\gamma_{1:k}) \propto \mathbb{P}(c=i|\gamma_{1:k-1})\mathbb{P}(\gamma_k|c=i,\gamma_{1:k-1}). \tag{9}$$

We assume, for simplicity, classifier outputs are statistically independent[1] and re-write Eq. (9) as

$$\lambda_k^i \propto \mathbb{P}(c=i|\gamma_{1:k-1})\mathbb{P}(\gamma_k|c=i). \tag{10}$$

Per the definition for λ_{k-1} (Eq. (2)) and $\mathbb{P}(\gamma_k|c=i)$ (Eq. (6)), λ_k^i assumes the following recursive form:

$$\lambda_k^i \propto \lambda_{k-1}^i\mathcal{L}_i(\gamma_k). \tag{11}$$

We now recall that γ_t (for each time step $t\in[1,k]$) is a random variable, making also λ_{k-1}^i and λ_k^i random variables. Thus, our problem is to infer $\mathbb{P}(\lambda_k|z_{1:k})$, where, according to Eq. (11), for each realization of the sequence $\gamma_{1:k}$, λ_k is a function of λ_{k-1} and γ_k.

We present our approach in Algorithm 1. At each time step t, a new image z_t is classified using multiple forward passes through a CNN with dropout, yielding a point cloud $\{\gamma_t\}$. Each forward pass gives a probability vector $\gamma_t\in\{\gamma_t\}$, which is used to compute the class likelihood $\mathcal{L}(\gamma_t)$, that is modeled as a Dirichlet distribution. In addition, we have a point cloud $\{\lambda_{t-1}\}$ from the previous step. We multiply all possible pairs of λ_{t-1}^i and $\mathcal{L}_i(\gamma_t)$, as in Eq. (11). Finally $N_{ss,n}$ pairs are chosen for the next step, in a sub-sampling algorithm that will be detailed in Section IV-B. We eventually get a point cloud $\{\lambda_t\}$ that approximates $\mathbb{P}(\lambda_t|z_{1:t})$.

```
Inputs:
    z_{1:k}: k images of an object.
    P(c = i) ∀ i = 1, ..., M : a prior for object class.
    L_i ∀ i = 1, ..., M: a classifier model.
    N_{ss,n} maximum points per time step
Outputs:
    A point cloud {λ_k} that approximates P(λ_k|z_{1:k}).
Initialize: λ_0^i = P(c = i)
for t = 1 : k do
    Classify image z_t, and produce a point cloud {γ_t}.
    for All possible γ_t and λ_{t-1} pairs: do
        for i = 1 : M do
            λ_t^i ∝ L_i(γ_t)λ_{t-1}^i
        end
    end
    Select randomly N_{ss,n} pairs to form {λ_t}
end
return {λ_k}
```

Algorithm 1: $\mathbb{P}(\lambda_k|z_{1:k})$ inference algorithm with sub-sampling.

We need to initialize the algorithm for the first image. Recalling Eq. (2), we define λ_1^i (first image) for class i and time $k=1$ as:

$$\lambda_1^i \doteq \mathbb{P}(c=i|\gamma_1). \tag{12}$$

[1]In this paper we do not consider viewpoint-dependent classifier models and thus model all $\gamma_{1:k}$ to be statistically independent from each other. We refer to our recent work [15] that relaxes this assumption while investigating complimentary aspects to this work.

Using Bayes law:

$$\mathbb{P}(c = i|\gamma_1) = \frac{\mathbb{P}(\gamma_1|c = i)\mathbb{P}(c = i)}{\mathbb{P}(\gamma_1)} \tag{13}$$

where $\mathbb{P}(c = i)$ is a prior probability of class i, $\mathbb{P}(\gamma_1)$ serves as a normalizing term, and $\mathbb{P}(\gamma_1|c = i)$ is the classifier model for class i. Per definition Eq. (6), Eq. (13) can be written as:

$$\lambda_1^i \propto \mathbb{P}(c = i)\mathcal{L}_i(\gamma_1), \tag{14}$$

thus λ_1^i is a function of prior $\mathbb{P}(c = i)$ and γ_1, and in the subsequent steps we can use the update rule of Eq. (11) to infer $\mathbb{P}(\lambda_k|z_{1:k})$.

Remark: There is a numerical issue where λ_k^i for sufficiently large k can practically become 0 or 1, preventing any possible change for future time steps. In our implementation, we overcome this by calculating $\log \lambda_k^i$ instead of λ_k^i.

In the next section we discuss the properties of $\mathbb{P}(\lambda_k|z_{1:k}))$, analyze the corresponding posterior uncertainty versus time, and consider two inference approaches that approximate this PDF.

A. Inference over the Posterior $\mathbb{P}(\lambda_k|z_{1:k})$

In this section we consider how the distribution $\mathbb{P}(\lambda_k|z_{1:k})$ develops and seek to find an inference method to track this distribution over time. As discussed in Section III, we consider all γ_t as random variables; hence, according to Eq. (11), $\mathbb{P}(\lambda_k|z_{1:k})$ accumulates all model uncertainty data from all $\mathbb{P}(\gamma_t|z_t)$ up until time step k, with $t \in [1, k]$.

Fig. 1 illustrates an example for inference of $\mathbb{P}(\lambda_k|z_{1:k})$ from $\mathbb{P}(\gamma_k|z_k)$ and $\mathbb{P}(\lambda_{k-1}|z_{1:k})$ using a known classifier model, considering three possible classes. Fig. 1a-1c present example distributions for the classifier model. Fig. 1d presents a point cloud that describes the distribution of λ_{k-1}. Fig. 1e presents $\mathbb{P}(\gamma_k|z_k)$ represented by a point cloud of γ_k instances. Each γ_k is projected via $\mathcal{L}(\gamma_k)$ to a different cloud in the simplex, presented in Fig. 1f. Finally, based on Eq. (11), the multiplication of points from Fig. 1d and 1f creates a $\{\lambda_k\}$ point cloud, shown in Fig. 1g. In the presented scenario, the spread of $\{\lambda_k\}$ (Fig. 1g) point cloud was smaller than $\{\lambda_{k-1}\}$ (Fig. 1d), because both point clouds $\{\lambda_{k-1}\}$ and $\{\mathcal{L}(\gamma_k)\}$ are near the same simplex edge. In general, classifier models with large parameters (see Eq. 5) create $\{\mathcal{L}(\gamma_t)\}$ point clouds that are closer to the simplex edge. In turn, the $\{\lambda_k\}$ point cloud (updated via Eq. (11)) will converge faster to a single simplex edge.

In this paragraph we discuss the behavior of $\mathbb{P}(\lambda_k)$, dependent on both λ_{k-1} and γ_k. The spread of $\{\lambda_k\}$ is indicative of accumulated model uncertainty, and is dependent on the expectation and spread of both $\{\lambda_{k-1}\}$ and $\{\gamma_k\}$. For specific realizations of λ_{k-1} and γ_k, as seen in Eq. (11), λ_k^i is a multiplication of λ_{k-1}^i and $\mathcal{L}_i(\gamma_k)$. Therefore, when $\mathcal{L}(\gamma_k)$ is within the simplex center, i,e. $\mathcal{L}_i(\gamma_k) = \mathcal{L}_j(\gamma_k)$ for all $i, j = 1, ..., M$, the resulting λ_k will be equal to λ_{k-1}. On the other hand, when $\mathcal{L}(\gamma_k)$ is at one of the simplex' edges, its effect on λ_k will be the greatest. Expanding to the probability $\mathbb{P}(\lambda_k|z_{1:k})$, there are several cases to consider.

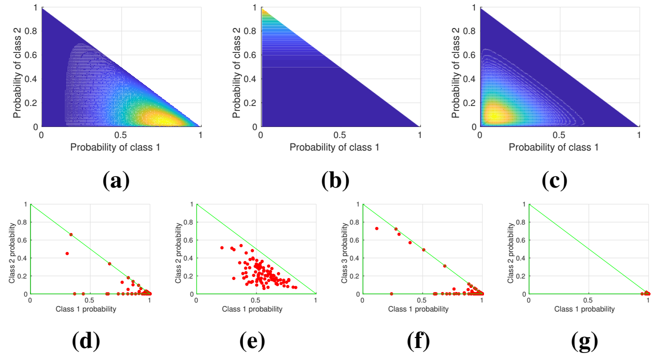

Figure 1: An example to illustrate the inference process of $\mathbb{P}(\lambda_k|z_{1:k})$. **(a)**, **(b)**, and **(c)** $\mathcal{L}_i$ classifier model for classes 1, 2 and 3, respectively, with higher probability zones presented in yellow. **(d)** distribution of λ_{k-1} from the previous step. Note that for $k = 1$, λ_0 is given by the prior $\mathbb{P}(c)$. **(e)** a point cloud $\{\gamma_k\}$ approximating $\mathbb{P}(\gamma_k|z_k)$ via multiple forward passes of the (CNN) classifier with dropout, given a new measurement z_k (an image) at current time step k. **(f)** The corresponding likelihood $\mathcal{L}(\gamma_k)$ for each $\gamma_k \in \{\gamma_k\}$ from **(e)**. Finally, multiplying λ_{k-1} and $\mathcal{L}(\gamma_k)$ (Eq. (11)) results in the point cloud shown in **(g)** representing a distribution over λ_k. λ_k's spread is smaller in this case than λ_{k-1}'s, as both $\mathcal{L}(\gamma_k)$ and $\mathbb{P}(\lambda_{k-1}|z_{k-1})$ are close to the same simplex corner.

If $\mathbb{P}(\lambda_{k-1}|z_{1:k-1})$ and $\{\mathcal{L}(\gamma_k)\}$ "agree" with each other, i.e. the highest probability class is the same, and both are far enough from the simplex center, the resulting $\mathbb{P}(\lambda_k|z_{1:k})$ will have a smaller spread compared to $\mathbb{P}(\lambda_{k-1}|z_{1:k-1})$ and its expectation will have the dominant class with a high probability. On the other hand, if $\mathbb{P}(\lambda_{k-1}|z_{1:k-1})$ and $\{\mathcal{L}(\gamma_k)\}$ "disagree" with each other, i.e. they are close to the same simplex corner, the spread of $\mathbb{P}(\lambda_k|z_{1:k})$ will become larger; an example for this case is illustrated in Fig. 2. In practice such a scenario can occur when an object of a certain class is observed from a viewpoint where it appears like a different class. If both $\mathbb{P}(\lambda_{k-1}|z_{1:k-1})$ and $\{\mathcal{L}(\gamma_k)\}$ are near the simplex center, the spread of $\mathbb{P}(\lambda_k|z_{1:k})$ will increase as well. Finally, if only one of $\mathbb{P}(\lambda_{k-1}|z_{1:k-1})$ and $\{\mathcal{L}(\gamma_k)\}$ is near the simplex center, $\mathbb{P}(\lambda_k|z_{1:k})$ will be similar to the one that is farther from the simplex center.

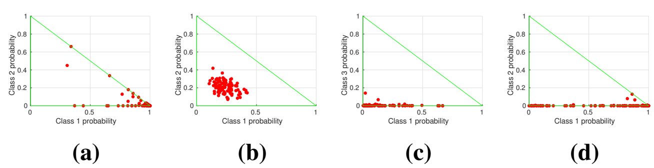

Figure 2: An example to illustrate a case where the posterior uncertainty *grows* with an additional image. The classifier model is the same as in Fig. 1, as well as the inference steps. **(a)** represents $\mathbb{P}(\lambda_{k-1}|z_{k-1})$. Here, in **(b)** the point cloud $\{\gamma_k\}$ is closer to class 3, compared to $\{\lambda_{k-1}\}$ cloud from **(a)** that is closer to class 1. The classifier model translates γ_k into $\mathcal{L}(\gamma_k)$ in **(c)**, projecting the point cloud around class 3, and thus after the multiplication in **(d)** the distribution is more spread out compared to **(a)**.

From $\mathbb{P}(\lambda_k|z_{1:k})$ we can infer the expectation $\mathbb{E}(\lambda_k)$ (computed as in Eq. (8)) and covariance matrix $Cov(\lambda_k)$ of λ_k. As $\mathbb{E}(\lambda_k)$ takes into account model uncertainty from each image, unlike existing approaches (e.g. [5]), we can achieve a posterior classification that is more resistant to possible aliasing. The covariance matrix $Cov(\lambda_k)$ represents the spread of λ_k, and in turn accumulates the model uncertainty from all images $z_{1:k}$. In general, lower $Cov(\lambda_k)$ values represent smaller λ_k spread, and thus higher confidence with the classification results. Practically, this can be used in a decision making context, where higher confidence answers are preferred. In this paper we compare between values of $Var(\lambda_k^i)$ for all classes $i = 1, ..., M$, as it is simpler to describe the uncertainty per class.

There is a correlation between the expectation $\mathbb{E}(\lambda_k)$ and $Cov(\lambda_k)$. The largest covariance values will occur when $\mathbb{E}(\lambda_k)$ is at the simplex' center. In particular, it is not difficult to show that the highest possible value for $Var(\lambda_k^i)$ for any i is 0.25; it can occur when $\lambda_k^i = 0.5$. In general, if $\mathbb{E}(\lambda_k)$ is close to the simplex' boundaries, the uncertainty is lower. Therefore, to reduce uncertainty, $\mathbb{E}(\lambda_k)$ should be concentrated in a single high probability class.

To the author's knowledge, the expression $\mathbb{P}(\lambda_k|z_{1:k})$, where the expression for λ_k is described in Eq. (11), has no known analytical solution. The next most accurate method available is multiplying all possible permutations of point clouds $\{\gamma_t\}$, for all images at times $t \in [1, k]$. This method is computationally intractable as the number of λ_k points grows exponentially. In the next section we propose a simple sub-sampling method to approximate this distribution and keep computational tractability.

B. Sub-Sampling Inference

As mentioned previously in section III, each measurement we receive a cloud of N_k probability vectors $\{(\gamma_k)^n\}_{n=1}^{N_k}$. Each probability vector is projected via the classifier model to a different point with the simplex, which provides a new point cloud $\{\mathcal{L}(\gamma_k)^n\}_{n=1}^{N_k}$. We assume that $\mathbb{P}(\lambda_{k-1}|z_{1:k-1})$ is described by a cloud of N_{k-1} points. Given the data for γ_k and λ_{k-1}, the most accurate approximation to $\mathbb{P}(\lambda_k|z_{1:k})$ is given by multiplying all possible pairs of λ_{k-1} and $\mathcal{L}(\gamma_k)$. Thus, $\mathbb{P}(\lambda_k|z_{1:k})$ is described with a cloud of $N_{k-1} \times N_k$ points. For subsequent steps the cloud size grows exponentially, making it computationally intractable. We address this problem by randomly sampling from the point cloud for λ_k a subset of $N_{ss,n}$ points and use them for the next time step. In practice, we keep $N_{ss,n}$ constant across all time steps, see line 16 in Algorithm 1.

V. Experiments

In this section we study our method in simulation and using real images fed into an AlexNet [16] CNN classifier. We used a PyTorch implementation of AlexNet for classification, and Matlab for sequential data fusion. Our hardware is an Intel i7-7700HQ CPU running at 2.8GHz, and 16GB of RAM. We compare between four different approaches:

1) `Method-`$\mathbb{P}(c|z_{1:k})$`-w/o-model`: Naive Bayes that infers the posterior of $\mathbb{P}(c|z_{1:k})$ where the classifier model is not taken into account (SSBF in [5]).
2) `Method-`$\mathbb{P}(c|z_{1:k})$`-w-model`: A Bayesian approach that infers the posterior of $\mathbb{P}(c|z_{1:k})$ and uses a classifier model; essentially using Eq. (11) with a known classifier model.
3) `Method-`$\mathbb{P}(\lambda_k|z_{1:k})$`-AP`: Inference of $\mathbb{P}(\lambda_k|z_{1:k})$ multiplying all possible combinations of λ_{k-1} and $\mathcal{L}(\gamma_k)$. Note that the number of combinations grows exponentially with k, thus the results are presented up until $k = 5$.
4) `Method-`$\mathbb{P}(\lambda_k|z_{1:k})$`-SS`: Inference of $\mathbb{P}(\lambda_k|z_{1:k})$ using the sub-sampling method.

Our proposed approaches are 3 and 4.

A. Simulated Experiment

This experiment is a simulation to demonstrate the algorithm's performance. This simulation is designed to emulate a scenario of a robot traveling in a predetermined trajectory and observing an object from multiple viewpoints. This object's class is one of three possible candidates. We infer the posterior over λ and display the results as expectation $\mathbb{E}(\lambda_k^i)$ and standard deviation per class i:

$$\sigma_i \doteq \sqrt{Var(\lambda_k^i)}. \tag{15}$$

This simulation is a study on the effect of using classifier model in the inference for highly ambiguous measurements. In addition, we analyze the uncertainty behavior for this scenario. We use a categorical uninformative prior of $\mathbb{P}(c = i) = 1/M$ for all $i = 1, ..., M$.

Each of the three classes has its own (known) classifier model Eq. (16), as shown in Figures 3a-3c. This classifier model is assumed Dirichlet distributed with the following hyperparameters θ_i for all $i \in [1, 3]$:

$$\begin{aligned} \theta_1 &= [6\ 1\ 1] \\ \theta_2 &= [2\ 7\ 2] \\ \theta_3 &= [1\ 1.5\ 2]\,. \end{aligned} \tag{16}$$

In this experiment the true class is 3. These hyperparameters were selected to simulate a case where the γ measurements are spread out (corresponds to ambiguous appearance of the class), thus leading to incorrect classification without a classifier model. The classifier model for this class $\mathcal{L}_3$ predicts highly variable γ's using the training data (Fig. 3c). The $\{\gamma_t\}$ point clouds for each $t \in [1, k]$ are different from each other (Fig. 3e), representing an object photographed by a robot from multiple viewpoints.

We simulate a series of 5 images. Each image at time step t has its own different $\mathbb{P}(\gamma_t|z_t)$. For the approaches that infer $\mathbb{P}(c|z_{1:k})$, we sample a single γ_t per image z_t for all $t \in [1, k]$ (Fig. 3f, also we present the γ_t order). This sample simulates the usual single classifier forward pass that is used. For our approaches we sample 10 γ_t's from each $\mathbb{P}(\gamma_t|z_t)$, except for the first step $t = 1$ where we sample 100 γ_1's. For `Method-`$\mathbb{P}(\lambda_k|z_{1:k})$`-SS` each $\{\lambda_t\}$ point cloud is capped at 100 points. The expectation of these generated measurements are presented in Fig. 3d, along with the cloud order. In Fig. 3e $\{\gamma_t\}$ point clouds for three different t's are presented in distinct colors. The input for methods 1 and 2 is shown in Fig. 3f, and some of the input for methods 3 and 4 is shown in Fig. 3e

Fig. 4 presents results obtained with our algorithm, in terms of expectation $\mathbb{E}(\lambda_k^i)$ and $\sqrt{Var(\lambda_k^i)}$ for each class i,

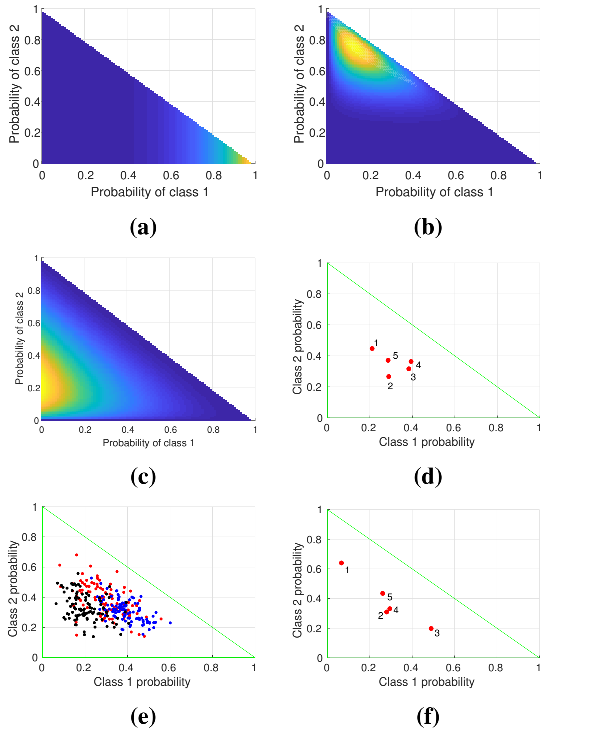

Figure 3: **(a)-(c)** Classifier likelihood model (Eq. (16)) for classes 1 to 3 respectively. Blue and orange colors correspond, respectively, to low and high probability values. **(d)** $\mathbb{E}(\gamma_t)$ for $t \in [1, 5]$ (i.e. 5 images). **(e)** Point cloud $\{\gamma_t\}$ for 3 images. **(f)** CNN classifier without dropout. In **(d)** and **(f)**, image indices are shown.

as a function of classifier measurements. In Fig. 4a and 4b we use a single sampled γ_t for z_t (see Fig. 3f), while in Fig. 4c and 4d we create a $\{\gamma_t\}$ point cloud for z_t (see Fig. 3e). In Fig. 4a and 4b results for Method-$\mathbb{P}(c|z_{1:k})$-w/o-model and Method-$\mathbb{P}(c|z_{1:k})$-w-model respectively. Without classifier model the results generally favor class 2 incorrectly, as the measurements tend to give that class the higher chances. With classifier models the results favor class 3, the correct class. Because the classifier model for class 3 is more spread out than for the other classes, γ's in the simplex middle (as in Fig. 3e) have higher $\mathcal{L}_3(\gamma)$ values than $\mathcal{L}_1(\gamma)$ and $\mathcal{L}_2(\gamma)$. While method Method-$\mathbb{P}(c|z_{1:k})$-w-model gives eventually correct classification results, it does not account for model uncertainty, i.e. uses a single classifier output γ obtained with a forward run through the classifier without dropout. In this simulation we sample a single γ from each point cloud to simulate this forward run.

Figs. 4c and 4d present the results for Method-$\mathbb{P}(\lambda_k|z_{1:k})$-SS and Method-$\mathbb{P}(\lambda_k|z_{1:k})$-AP, expectation and standard deviation respectively. Throughout the scenario class 3 has the highest probability correctly, and the deviation drops as more measurements are introduced. Compared to Fig. 4b where class 3 has high probability only at time step $t = 3$, in Fig. 4c class 3 is the most probable from time step $t = 1$. Both Method-$\mathbb{P}(\lambda_k|z_{1:k})$-SS and Method-$\mathbb{P}(\lambda_k|z_{1:k})$-AP behave similarly. Note that class 1 has much smaller deviation than the other two because its probability is close to 0 through the entire scenario.

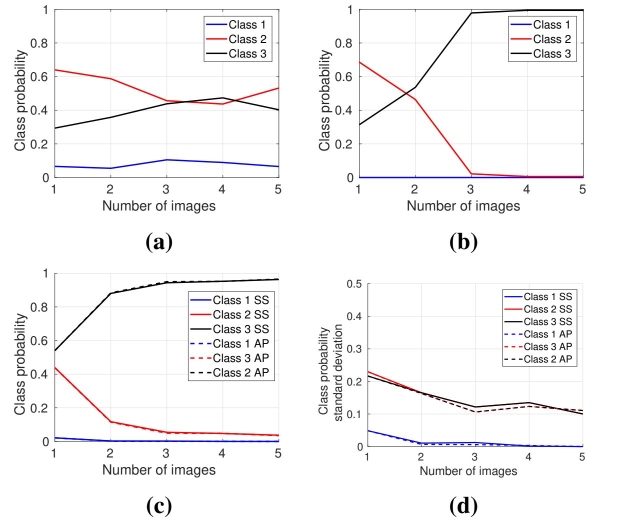

for both of our methods.

Figure 4: **(a)-(c)** Posterior class probabilities: **(a)** Method-$\mathbb{P}(c|z_{1:k})$-w/o-model; **(b)** Method-$\mathbb{P}(c|z_{1:k})$-w-model; **(c)** $\mathbb{P}(c|z_{1:k})$ calculated via expectation (8) for Method-$\mathbb{P}(\lambda_k|z_{1:k})$-SS and Method-$\mathbb{P}(\lambda_k|z_{1:k})$-AP; **(d)** presents the posterior standard deviation Eq. (15)

Fig. 5 presents the development of $\{\lambda_k\}$ point clouds for Method-$\mathbb{P}(\lambda_k|z_{1:k})$-SS at different time steps. Those figures show the gradual decrease in $\{\lambda_k\}$'s spread, coinciding with the corresponding standard deviation at Fig. 4d.

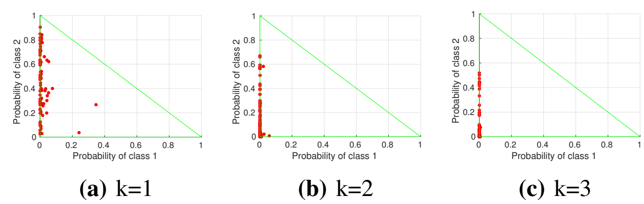

Figure 5: The figure depicts the evolution of the $\{\lambda_k\}$ point cloud, as calculated by Method-$\mathbb{P}(\lambda_k|z_{1:k})$-SS, for different time instances k.

B. Experiment with Real Images

Our algorithm is tested using a series of images of an object (space heater) with conflicting classifier outputs when observed from different viewpoints. This corresponds to a scenario where a robot in a predetermined path observes an object that is obscured by occlusions and different lighting conditions. The experiment presents our algorithm's robustness to these difficulties in classification, and addressing them is important for real-life robotic applications.

The database photographed is a series of 10 images of a space heater with artificially induced blur and occlusions. Each of the images is run through an AlexNet convolutional neural network [16] with 1000 possible classes. Similar to Section V-A, we use an uninformative classifier prior on $\mathbb{P}(c)$ with $\mathbb{P}(c = i) = 1/M$ for all $i = 1, ..., M$ classes. Our algorithm is used to fuse the classification data into a posterior distribution of the class probability and infer deviation for each class. As in the previous section, we present results with and without classifier model. Fig. 6 presents four of the dataset images, exhibiting occlusions, blur and different colored filters in a monotone environment.

(a) (b) (c) (d)

Figure 6: Four of the 10 images used in the dataset with occlusions and different viewpoints. Blurring and colored filters were introduced to some images artificially.

We compare between the same methods that are used in the previous sub-sections. For Method-$\mathbb{P}(c|z_{1:k})$-w/o-model and Method-$\mathbb{P}(c|z_{1:k})$-w-model, we forward the images through the classifier without dropout and use a single output γ for each image. For Method-$\mathbb{P}(\lambda_k|z_{1:k})$-SS, we run each image 10 times through the classifier with dropout, producing a point cloud $\{\gamma\}$ per image. The cap for number of λ_k points with Method-$\mathbb{P}(\lambda_k|z_{1:k})$-SS is 100. For Method-$\mathbb{P}(\lambda_k|z_{1:k})$-AP method, we present results only for the first five images as the calculations become infeasible due to the exponential complexity.

As AlexNet has 1000 possible classes (one of them is ”Space Heater”), it is difficult to clearly present results for all of them. Because we wish to compare between the most likely classes, we select 3 likely classes by averaging all γ classifier outputs and selecting the three with highest probability. The probabilities for those classes are then normalized, and utilized in the scenario. All other classes outside those three are ignored. We require a classifier model for each class; assuming the classifier model is Dirichlet distributed, we classified multiple images unrelated to the scenario for each class with the same AlexNet classifier but without dropout. The classifier produced multiple γ’s, one per image, and via a Maximum Likelihood Estimator [17] we inferred the Dirichlet hyperparameters for each class $i \in [1, 3]$. The classifier model $\mathbb{P}(\gamma_k|c = i) = Dir(\gamma_k; \theta_i)$ was used with the following hyperparameters θ_i:

$$\begin{aligned}\theta_1 &= [5.103\ 1.699\ 1.239]\\ \theta_2 &= [0.143\ 208.7\ 5.31]\\ \theta_3 &= [0.993\ 14.31\ 25.21]\end{aligned} \tag{17}$$

In this experiment, class 1 is the correct class (i.e. ”Space Heater”). Fig. 7 presents the simplex representation of the classifier model per class, and a normalized simplex of classifier outputs for three high probability classes, similarly to Fig. 3. The classifier model for class 1 is much more spread than the other two (Fig. 7a), therefore the likelihood of measurements within a larger area will be higher for this class. Interestingly, the classifier model for class 3 predicts $\mathbb{P}(\gamma_k|c = 3)$ will be between classes 2 and 3 (Fig. 7c). Fig. 7e presents 4 of the 10 $\{\gamma_t\}$ point clouds used in the scenario. Fig. 7d presents the expectation of each $\{\gamma_t\}$ point cloud for $t \in [1, 10]$. Fig. 7f presents classifier outputs without dropout, i.e. a single γ_t per image. Both Fig. 7d and 7f have indices that represent the images order.

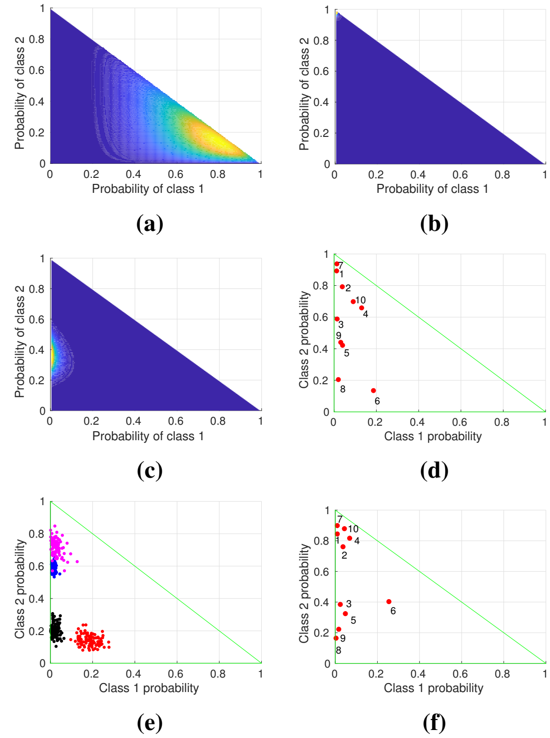

Figure 7: A simplex representation of the classifier model for **(a)** class 1, **(b)** class 2, and **(c)** class 3. In **(b)**, note the distribution is very tight centered at the top left corner of the simplex. **(d)** $\mathbb{E}(\gamma_t)$ for $t \in [1, 10]$ (i.e. 10 images). **(e)** Pointcloud $\{\gamma_t\}$ for 4 images. **(f)** CNN classifier output without dropout. In **(d)** and **(f)**, image indices are shown.

Fig. 8 presents the classification results for all the methods presented. Fig. 8a and 8b show results for Method-$\mathbb{P}(c|z_{1:k})$-w/o-model and Method-$\mathbb{P}(c|z_{1:k})$-w-model respectively. Without a classifier model, i.e. the former method, incorrectly indicates class 2 as the most likely, because the classifier outputs often show class 2 as the most likely (see Fig. 7f). With a classifier model, the results jump between classes 1 and 3 as most probable. This can be explained by the likelihood vector $\mathcal{L}$ from Eq. (17) that projects the γ’s from different images approximately to different simplex edges (e.g. γ_2 and γ_4 for class 1, and γ_3 and γ_5 for class 3).

Figs. 8c and 8d present results for Method-$\mathbb{P}(\lambda_k|z_{1:k})$-SS and Method-$\mathbb{P}(\lambda_k|z_{1:k})$-AP, expectation and standard deviation respectively. Fig. 8c presents class 1 as most likely correctly in both methods from $k = 2$ onwards, and the results are smoother than in Fig. 8b because our algorithm takes into account multiple realizations of γ_1 to γ_{10} - we recall that for each image we use a point cloud of γ’s. In addition, we can reason about the standard deviation of λ_k, representing the posterior uncertainty, as seen in Fig. 8d. Note that starting from the 4th image, the uncertainty *increases*, as later measurement likelihoods do not agree with λ_{k-1} about the most likely class at those time steps, similar to the example presented in Fig. 2.

Fig. 9a presents the computational time comparison be-

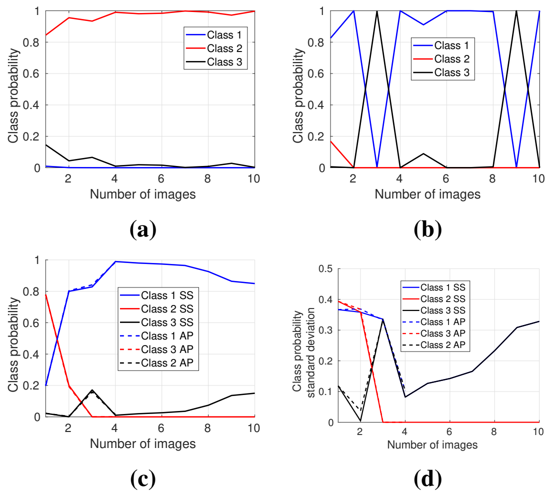

Figure 8: **(a)-(c)** Posterior class probabilities: **(a)** Method-$\mathbb{P}(c|z_{1:k})$-w/o-model; **(b)** Method-$\mathbb{P}(c|z_{1:k})$-w-model; **(c)** $\mathbb{P}(c|z_{1:k})$ calculated via expectation (8) for Method-$\mathbb{P}(\lambda_k|z_{1:k})$-SS and Method-$\mathbb{P}(\lambda_k|z_{1:k})$-AP; **(d)** presents the posterior standard deviation Eq. (15) for both of our methods.

tween those two methods for the scenario presented in this section, including different number of samples $N_{ss,n}$ per time step. Importantly, the results for Method-$\mathbb{P}(\lambda_k|z_{1:k})$-SS are similar to Method-$\mathbb{P}(\lambda_k|z_{1:k})$-AP while offering significantly shorter computational times. Note that the computational time per step is constant as well for Method-$\mathbb{P}(\lambda_k|z_{1:k})$-SS. Fig. 9b presents mean square error (MSE) of Method-$\mathbb{P}(\lambda_k|z_{1:k})$-SS compared to Method-$\mathbb{P}(\lambda_k|z_{1:k})$-AP, as a function of $N_{ss,n}$. As expected, larger $N_{ss,n}$ values produce lower MSE.

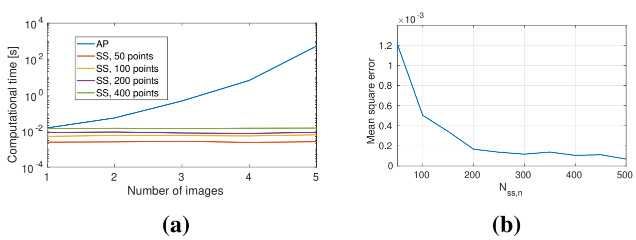

Figure 9: (a) Computational time comparison between Method-$\mathbb{P}(\lambda_k|z_{1:k})$-AP and Method-$\mathbb{P}(\lambda_k|z_{1:k})$-SS per time step. The figure presents computational times for $N_{ss,n} \in \{50, 100, 200, 400\}$ points per time step for Method-$\mathbb{P}(\lambda_k|z_{1:k})$-SS. (b) The statistical mean square error of Method-$\mathbb{P}(\lambda_k|z_{1:k})$-SS as a function of $N_{ss,n} \in [50, 500]$ relative to Method-$\mathbb{P}(\lambda_k|z_{1:k})$-AP.

VI. Conclusions

We proposed a method that infers a distribution over posterior class probabilities with a measure of uncertainty using a modern, deep learning classifier. As opposed to state of the art, our approach enables quantification of uncertainty in posterior classification given all data thus far, and as such is important for robust classification, object-level perception and safe autonomy. In particular, we showed that the current posterior class probability vector is a function of the previous, accounting for model uncertainty. We used a sub-sampling approximation to obtain a point cloud that approximates the function's distribution. Our approach is studied in simulation, and with real images fed into a deep learning classifier, providing classification posterior along with uncertainty estimates for each time instant. Future research might explore active classification aspects via belief space planning.

VII. Acknowledgments

The authors thank Yuri Feldman from the Technion's Department of Computer Science for numerous useful discussions.

References

[1] Yarin Gal and Zoubin Ghahramani. Bayesian convolutional neural networks with bernoulli approximate variational inference. *arXiv preprint arXiv:1506.02158*, 2016.

[2] Yarin Gal and Zoubin Ghahramani. Dropout as a bayesian approximation: Representing model uncertainty in deep learning. In *Intl. Conf. on Machine Learning (ICML)*, 2016.

[3] Pavel Myshkov and Simon Julier. Posterior distribution analysis for bayesian inference in neural networks. *Advances in Neural Information Processing Systems (NIPS)*, 2016.

[4] Adam Coates and Andrew Y Ng. Multi-camera object detection for robotics. In *Robotics and Automation (ICRA), 2010 IEEE International Conference on*, pages 412–419. IEEE, 2010.

[5] Shayegan Omidshafiei, Brett T Lopez, Jonathan P How, and John Vian. Hierarchical bayesian noise inference for robust real-time probabilistic object classification. *arXiv preprint arXiv:1605.01042*, 2016.

[6] N. Atanasov, B. Sankaran, J.L. Ny, G. J. Pappas, and K. Daniilidis. Nonmyopic view planning for active object classification and pose estimation. *IEEE Trans. Robotics*, 30:1078–1090, 2014.

[7] Beipeng Mu, Shih-Yuan Liu, Liam Paull, John Leonard, and Jonathan How. Slam with objects using a nonparametric pose graph. In *IEEE/RSJ Intl. Conf. on Intelligent Robots and Systems (IROS)*, 2016.

[8] WT Teacy, Simon J Julier, Renzo De Nardi, Alex Rogers, and Nicholas R Jennings. Observation modelling for vision-based target search by unmanned aerial vehicles. In *Intl. Conf. on Autonomous Agents and Multiagent Systems (AAMAS)*, pages 1607–1614, 2015.

[9] Javier Velez, Garrett Hemann, Albert S Huang, Ingmar Posner, and Nicholas Roy. Modelling observation correlations for active exploration and robust object detection. *J. of Artificial Intelligence Research*, 2012.

[10] T. Patten, M. Zillich, R. Fitch, M. Vincze, and S. Sukkarieh. Viewpoint evaluation for online 3-d active object classification. *IEEE Robotics and Automation Letters (RA-L)*, 1(1):73–81, January 2016.

[11] V. Indelman, E. Nelson, J. Dong, N. Michael, and F. Dellaert. Incremental distributed inference from arbitrary poses and unknown data association: Using collaborating robots to establish a common reference. *IEEE Control Systems Magazine (CSM), Special Issue on Distributed Control and Estimation for Robotic Vehicle Networks*, 36(2):41–74, 2016.

[12] Hugo Grimmett, Rudolph Triebel, Rohan Paul, and Ingmar Posner. Introspective classification for robot perception. *Intl. J. of Robotics Research*, 35(7):743–762, 2016.

[13] Alex Kendall and Roberto Cipolla. Modelling uncertainty in deep learning for camera relocalization. *arXiv preprint arXiv:1509.05909*, 2015.

[14] Alex Kendall and Yarin Gal. What uncertainties do we need in bayesian deep learning for computer vision? *arXiv preprint arXiv:1703.04977*, 2017.

[15] Yuri Feldman and Vadim Indelman. Bayesian viewpoint-dependent robust classification under model and localization uncertainty. In *IEEE Intl. Conf. on Robotics and Automation (ICRA)*, 2018.

[16] Alex Krizhevsky, Ilya Sutskever, and Geoffrey E Hinton. Imagenet classification with deep convolutional neural networks. In *Advances in neural information processing systems*, pages 1097–1105, 2012.

[17] Jonathan Huang. Maximum likelihood estimation of dirichlet distribution parameters. *CMU Technique Report*, 2005.